THE JOURNAL OF BIOLOGICAL CHEMISTRY VOL. 288, NO. 9, pp. 6488–6497, March 1, 2013

Inactivation of Max-interacting Protein 1 Induces Renal Cilia Disassembly through Reduction in Levels of Intraflagellar Transport 20 in Polycystic Kidney*

Received for publication, August 25, 2012, and in revised form, January 10, 2013 Published, JBC Papers in Press, January 13, 2013, DOI 10.1074/jbc.M112.413302

Je Yeong Ko[‡1], Kyung Hyun Yoo[‡1,2], Seon Ah Song[‡], Do Yeon Kim[‡], Hyun Kyung Kong[‡], Curie Ahn[§], Han Woong Lee[¶], Duk-Hee Kang[‖], Goo Taeg Oh[**], and Jong Hoon Park[‡3]

From the [‡]Department of Biological Science, Sookmyung Women's University, Seoul 140-742, Republic of Korea, the [§]Department of Internal Medicine, Seoul National University College of Medicine, Seoul 110-744, Republic of Korea, the [¶]Department of Biochemistry, Yonsei University, Seoul 120-749, Republic of Korea, the [‖]Department of Internal Medicine, School of Medicine and [**]Department of Biological Science, Ewha Womans University, Seoul 120-750, Republic of Korea

Background: Renal cilia defects such as cilia disassembly cause polycystic kidney disease.
Results: Decrease of Mxi1 induces renal cilia disassembly via reduction in levels of Ift20 and activates *p*-ERK.
Conclusion: Inactivation of Mxi1 induces polycystic kidney through renal cilia disassembly.
Significance: This cilia disassembly mechanism induced by Mxi1 inactivation in polycystic kidney is expected to be new model for renal cystogenesis.

Cilia in ciliated cells consist of protruding structures that sense mechanical and chemical signals from the extracellular environment. Cilia are assembled with variety molecules via a process known as intraflagellar transport (IFT). What controls the length of cilia in ciliated cells is critical to understand ciliary disease such as autosomal dominant polycystic kidney disease, which involves abnormally short cilia. But this control mechanism is not well understood. Previously, multiple tubular cysts have been observed in the kidneys of max-interacting protein 1 (*Mxi1*)-deficient mice aged 6 months or more. Here, we clarified the relationship between Mxi1 inactivation and cilia disassembly. Cilia phenotypes were observed in kidneys of *Mxi1*-deficient mice using scanning electron microscopy to elucidate the effect of Mxi1 on renal cilia phenotype, and cilia disassembly was observed in *Mxi1*-deficient kidney. In addition, genes related to cilia were validated *in vitro* and *in vivo* using quantitative PCR, and *Ift20* was selected as a candidate gene in this study. The length of cilium decreased, and *p*-ERK level induced by a cilia defect increased in kidneys of *Mxi1*-deficient mice. Ciliogenesis of *Mxi1*-deficient mouse embryonic fibroblasts (MEFs) decreased, and this abnormality was restored by *Mxi1* transfection in *Mxi1*-deficient MEFs. We confirmed that ciliogenesis and *Ift20* expression were regulated by Mxi1 *in vitro*. We also determined that Mxi1 regulates *Ift20* promoter activity via Ets-1 binding to the *Ift20* promoter. These results indicate that inactivating Mxi1 induces ciliary defects in polycystic kidney.

Most eukaryotic cells contain organelles known as cilia, which are antenna-like projections extending from the cell body. Nonmotile, primary cilia may be sensory cellular organelles that coordinate cellular signaling pathway including cell division and differentiation (1). A single primary cilium emanates from the basal body in kidney cells and exhibits a 9 + 0 (nine sets of microtubule doublets and no singlet microtubule in the center) axoneme microtubule structure (2). The process of intraflagellar transport (IFT)[4] is responsible for building and maintaining the structure and function of primary cilia (3). Central to the functional basis of IFT is its ability to traffic various ciliary protein cargo (4). IFT particles are divided into two groups termed complex A and B. Components of IFT complex A function are related to retrograde IFT (Ift144/140/139/122), whereas components of IFT complex B function are related to anterograde IFT (Ift172/88/81/80/74/57/52/46/27/20) (5).

Recent research has demonstrated that cilia play a crucial role regulating vertebrate developmental pathways and tissue homeostasis, and defects in genes involved in primary cilia assembly or function are associated with diseases such as polycystic kidney disease (PKD) (6–10). Autosomal dominant PKD (ADPKD), which is one of the most common human monogenic diseases, is a life-threatening genetic disease in which epithelial-lined cysts develop extensively in the kidneys resulting in renal failure (11–15). PKD is related to abnormal proliferation of renal epithelial cells with ciliary defects. In addition, ADPKD is one of a number of human genetic diseases that are rooted in defects in cilia formation, maintenance, or function (16–18).

Max-interacting protein 1 (Mxi1), which is an antagonist of the c-Myc oncogene, is a transcription factor related to cellular

* This work was supported by Grants 2011-0031220 and 2011-0019452 from the Bio and Medical Technology Development Program of the National Research Foundation of Korea.
[1] Both authors contributed equally to this work.
[2] Present address: National Institutes of Health (NIH), 9000 Rockville Pike, Bethesda, MD 20892.
[3] To whom correspondence should be addressed. Tel.: 82-2-710-9414; Fax: 82-2-2077-7322; E-mail: parkjh@sookmyung.ac.kr.

[4] The abbreviations used are: IFT, intraflagellar transport; ADPKD, autosomal dominant PKD; Ets-1, E26 avian leukemia oncogene 1; MEF, mouse embryonic fibroblast; mIMCD-3, mouse inner medullary collecting duct; Mxi1, max-interacting protein 1; PKD, polycystic kidney disease.

growth and differentiation (19–21). The Mad2 protein encoded by the *Mxi1* gene is a basic helix-loop-helix leucine zipper (22). Deletion or rearrangement of the *Mxi1* gene causes several types of cancer in humans including prostate tumors, renal cell carcinoma, and endometrial cancers (22, 23). Mice lacking *Mxi1* exhibit progressive, multisystem abnormalities including polycystic kidney (24). Previously, we reported multiple cysts in the kidneys of *Mxi1*-deficient mouse aged 6 months and older (25). Also, the common characteristics of polycystic kidney such as inflammation, fibrosis, and increase of renal cell proliferation were observed in *Mxi1*-deficient kidney (22, 26). Based on these previous studies, *Mxi1*-deficient mice are a suitable model to study PKD.

Here, we show that inactivating Mxi1 affects ciliogenesis *in vivo* and *in vitro* by down-regulating Ift20. Additionally, the *p*-ERK level was increased in cilia-defective models by the inactivation of *Mxi1*. To investigate the relationship between Mxi1 and Ift20, various transcription factors binding to the *Ift20* promoter region were screened using the TRANSFAC database. The results confirmed that Ets-1 acts as a mediator involved in the relationship between Mxi1 and Ift20. These results suggest that inactivation of Mxi1 induces renal cilia disassembly through Ift20 reduction in polycystic kidneys.

EXPERIMENTAL PROCEDURES

Sample Preparation—Renal tissue was isolated from 9-month-old *Mxi1*-deficient mice and age-matched control mice. For histological analysis, tissues were fixed in freshly prepared 4% paraformaldehyde in PBS, dehydrated in graded ethanol, cleared in xylene, and embedded in paraffin. Kidney tissues were taken from sacrificed mice and immediately stored in 2.5% glutaraldehyde for scanning electron microscopy.

Cell Culture—Wild-type and *Mxi1*-deficient mouse embryonic fibroblasts (MEFs) were isolated from E13.5 mouse embryos. Briefly, embryos were mechanically fragmented and then incubated with trypsin (0.25% in PBS, pH 7.5) at 37 °C for 15–20 min with a magnetic stirrer. After 10 min of centrifugation at 1800 rpm, the pellets were resuspended in Dulbecco's modified Eagle's medium (DMEM) without fetal bovine serum (FBS) and centrifuged for 10 min at 1800 rpm. After three washes, the cell suspension was distributed in a culture dish containing complete DMEM with 10% FBS. Inner medullary collecting duct (mIMCD-3) cells were cultured in DMEM and Ham's F12 medium supplemented with 10% FBS. Cells were grown at 37 °C in a humidified atmosphere containing 5% CO_2. To induce ciliogenesis, mIMCD-3 cells were maintained at confluence for 5 days (27). MEFs were maintained at serum starvation for 48 h to induce ciliogenesis (28).

Mxi-1 and Ets-1 Expression Vector—The *Mxi1* expression vector, pCMV Tag2B (Stratagene), was constructed by cloning *Mxi1* cDNA isolated from mIMCD-3 cells. *Mxi1* coding sequence constructs were made by PCR amplification with the following primers: upstream, 5′-GATCGGATCC (BamHI) ATGCCGAGCCCCCGG-3′ and downstream, 5′-TCGACTCGAG (XhoI) CTAGGACGCGAAGGAGG-3′. The *Ets-1* expression vector, also pCMV Tag2B, was constructed by cloning *Ets-1* cDNA isolated from mIMCD-3 cells. *Ets-1* coding sequence constructs were made by PCR amplification with the following primers: upstream, 5′-ATTTGCGGCCGC (NotI) ATGAAGGCGGCCGTCGAT-3′ and downstream, 5′-CGCGGATCCCTA (BamHI) GTCAGCATCCGGCTTTACAT-3′.

Transient Transfection and siRNA Treatment—Transient transfection of *Mxi1* and *Ets-1* was performed with following materials. Cells were subcultured 1 day before and transfected using FuGENE 6 Transfection Reagent (Roche Applied Science). Cells were transfected with *Mxi1* and *Ets-1* small interfering RNA (siRNA; Santa Cruz Biotechnology) using Lipofectamine RNAi MAX (Invitrogen), according to the manufacturer's protocol.

Immunofluorescence Microscopy—Cells for immunofluorescence microscopy were grown on acid-washed glass coverslips. The cells were fixed for 10 min in 4% paraformaldehyde in PBS. Five- to 10-μm-thick paraffin sections were used for immunofluorescence microscopy and incubated with primary antibodies overnight at 4 °C. The primary antibodies used included acetylated anti-tubulin (Sigma-Aldrich). The cells were then washed three times and incubated with a 1:1000 dilution of FITC-conjugated anti-mouse IgG (Vector Laboratories) secondary antibody for 1 h at room temperature. The cells were then mounted with Vectashield (Vector Laboratories) and visualized by fluorescence microscopy. Counterstaining was carried out with DAPI.

Reporter Constructs and Luciferase Assay—Mouse genomic DNA was isolated from wild-type mouse embryos using BD Vacutainers. The 5′-flanking region of the mouse *Ift20* gene was amplified by PCR using specific primers. The synthetic linkers and restriction sites for XhoI (CCGCTCGAG) and HindIII (GGGAAGCTT) are indicated in uppercase. The primers used were: 0.5 kb forward, 5′-CCGCTCGAGCACCCCTCCTCTTCTGAAAAACT-3′ and 1.0 kb forward, 5′-CCGCTCGAGAGAAACCCAAGTGACTAGGCTTG-3′; the reverse primer for all constructs except for 0.5kb-1.0kb, 5′-GGGAAGCTTAGCACCAGCATCCGCCCACCCTGCGG-3′ and the reverse primer for 0.5kb-1.0kb, 5′-GGGAAGCTTTGGCGGGAGAGCAGCCTACACT-3′. A series of 5′-deletion constructs were cloned into the pGL3-basic vector (Promega). For site-directed mutagenesis, the pGL3-basic/0.5-kb cloned vector was used as a template with the QuikChange® Site-Directed Mutagenesis Kit (Stratagene). The mutated region was the same as the Ets-1 mutant probe used in the shift assay. Luciferase plasmids and a pSV-β-galactosidase control vector were cotransfected into mIMCD-3 cells, *Mxi1* transiently overexpressed, and *Ets-1* transiently overexpressed mIMCD-3 cells with the FuGENE 6 Transfection Reagent. After 2 days, the cells were washed with PBS and harvested in 500 μl of 1× Passive Lysis Buffer (Promega). Supernatants were mixed with luciferase reagent (Promega), and luciferase activity was measured using a luminometer (Aureon Biosystems) as described in the manufacturer's protocol.

Quantitative PCR—Total RNA was extracted using a Nucleospin® Kit (Macherey-Nagel) according to the manufacturer's instructions, and cDNA was synthesized using Moloney murine leukemia virus reverse transcriptase (Promega) according to the manufacturer's instructions. qPCR was conducted using the qPCR SYBR Green kit (Qiagen). Primer sequences for qPCR are presented in Table 1.

TABLE 1
Primer sequences

Primer (qPCR)[a]	5′→3′
β-Actin (F)	GACGATGCTCCCCGGGCTGTATTC
β-Actin (R)	TCTCTTGCTCTGGGCCTCGTCACC
Mxi1 (F)	CGGATTCAGAGCGAGAGGAGATT
Mxi1 (R)	AGGCTGCTGTGGTCGTCAAGGTC
Ift20 (F)	GGATGCTGGTGCTTCTGGACTC
Ift20 (R)	GCTCTGCGGCCCTGACGACTGT
Ift88 (F)	TGGTCAGCCCGCTCCTCCTC
Ift88 (R)	ACCCGTGTCATTCTCCAACTCCTC
Kif3α (F)	CCAGCCTCGCCCCCAAACC
Kif3α (R)	CCGGCACCTAACCACCACCTTC

[a] F, forward; R, reverse.

Western Blotting—Proteins were separated on polyacrylamide gels and transferred to PVDF membranes (Amersham Biosciences). The primary antibodies used were anti-cytoskeletal actin (Bethyl Laboratories), anti-ERK, anti-*p*-ERK (Cell Signaling Technology), *Mxi1* (Santa Cruz Biotechnology), Ets-1 (Novus), and Ift20 (Abcam). Blots were incubated with primary antibodies overnight at 4 °C. Blots were incubated with horseradish peroxidase-conjugated secondary antibody (Upstate Biotechnology, 1:5000) for 1 h at room temperature. Immunoreactive complexes were visualized using ECL reagents (Amersham Biosciences).

Supershift Assay and Isolation of Nuclear Extracts—Nuclear extracts of mIMCD-3 cells were prepared using a Nuclear Extraction Kit (Affymetrix) according to the manufacturer's protocol. The sequences of oligonucleotides used in the supershift assay were: Ets-1 wild-type probe, 5′-TCCTTC-TACTTCCGGGTTCGG-3′ and Ets-1 mutant probe, 5′-TCCTTCTACAAAAGGGTTCGG-3′. Probes were labeled with [γ-^{32}P]ATP using T4 polynucleotide kinase (Takara), followed by purification on a Sephadex G-50 column (Roche Applied Science). Nuclear extracts were preincubated with unlabeled probe (competitor) for 90 min at room temperature for the competitive binding assay. Nuclear extracts were preincubated with antibodies against Ets-1 and IgG for 90 min at room temperature for the supershift assay. All antibodies for the supershift assay were purchased from Santa Cruz Biotechnology. Samples were loaded on polyacrylamide gel in 0.5× TBE buffer for 3 h at 180 V. The dried gels were exposed to film and detected with a FLA7000 (Fuji film).

Statistical Analysis—Data were described as mean ± S.D. and analyzed by a paired *t* test. The paired *t* test was performed by InStat software (GraphPad). For analysis, p value < 0.05 was considered statistically significant.

RESULTS

Influence of Mxi1 Inactivation on Cilia Assembly—To confirm the effect of *Mxi1* deletion on cilia assembly, we evaluated the length of the primary cilia in kidneys of *Mxi1*-deficient and wild-type mice by scanning electron microscopy (Fig. 1*A*). Cilia formation was normal in wild-type kidneys (Fig. 1*A*, *a–c*), whereas cells with defective and truncated cilia were observed in *Mxi1*-deficient mice (Fig. 1*A*, *d–f*). A comparison of the length of the cilium in *Mxi1*-deficient kidneys with that of the wild-type kidney ($n = 20$, 3.284 ± 0.697 μm) revealed that cilia in the *Mxi1*-deficient kidney ($n = 15$, 1.84 ± 0.663 μm) were much shorter than those in the wild-type (Fig. 1*B*). Next, we investigated the phenotype of cilia in cyst-lining cells of the *Mxi1*-deficient kidney compared with that in the wild-type (Fig. 1*C*). Results from immunofluorescence using an antibody against acetylated α-tubulin, known as a primary cilia-specific marker, showed that cilia still formed in the cyst-lining cells (Fig. 1*C*, *b* and *c*), but their phenotype was abnormal compared with that in wild-type kidney (Fig. 1*C*, *a*). Cilia formed in wild-type kidney were normally protruded to lumen and maintained normal cilia length. However, cilia formed in *Mxi1*-deficient kidney did not have extended form to lumen with short length. In addition, the B-Raf/MEK/ERK pathway was confirmed in kidney of *Mxi1*-deficient mice. Because decrease of intracellular calcium level in polycystic kidney with cilia defects induce cAMP level that results in activation of B-Raf/MEK/ERK pathway (29). The *p*-B-Raf, *p*-MEK, and *p*-ERK level increased in the cilia-defective kidney induced by *Mxi1* inactivation compared with that in controls (Fig. 1*D*). These results show that inactivation of *Mxi1* induces truncated cilia and activation of B-Raf/MEK/ERK pathway in the kidney.

Influence of Mxi1 Inactivation on Ciliogenesis in MEFs—We imaged ciliated cells in $Mxi1^{+/+}$ and $Mxi1^{-/-}$ MEFs to confirm whether ciliogenesis was affected by the *Mxi1* gene in MEFs. In normal cells, the proper ciliogenesis occurred in one cell, so one cilium is localized to one cell. Consistent with this, many $Mxi1^{+/+}$ MEFs have cilia in each cell (Fig. 2*A*). However, ciliated cells of $Mxi1^{-/-}$ MEFs was reduced compared with $Mxi1^{+/+}$ MEFs (Fig. 2*A*). These results suggest that ciliogenesis was inhibited in $Mxi1^{-/-}$ MEFs compared with those in $Mxi1^{+/+}$ MEFs. Quantification of ciliogenesis was indicated in Fig. 2*B*. The percentage of ciliated cells decreased in $Mxi1^{-/-}$ MEFs ($n = 11$, 30.151 ± 16.674%) compared with those in $Mxi1^{+/+}$ MEFs ($n = 11$, 71.969 ± 20.84%). Additionally, the *p*-ERK level increased in $Mxi1^{-/-}$ MEFs compared with that in $Mxi1^{+/+}$ MEFs (Fig. 2*C*). These results indicated that *Mxi1* regulates ciliogenesis and the *p*-ERK level in MEFs.

Validation of Gene Expression Related to Ciliogenesis in Mxi1-deficient Kidneys and MEFs—To identify the expression pattern of the IFT family involved in ciliogenesis, we evaluated the expression of *Ift20*, *Ift88*, and *Kif3α* in *Mxi1*-deficient kidneys using qPCR (Fig. 3*A*). *Ift20* (0.521 ± 0.394), *Ift88* (0.771 ± 0.212), and *Kif3α* (0.633 ± 0.159) were down-regulated in *Mxi1*-deficient mice with polycystic kidneys. We also confirmed expression of these genes in MEFs (Fig. 3*B*). *Ift20* (0.428 ± 0.125), *Ift88* (0.658 ± 0.337), and *Kif3α* (0.684 ± 0.078) were down-regulated in *Mxi1*-deficient MEFs compared with that in controls. Among these genes, *Ift20* expression decreased significantly in the *Mxi1*-deficient kidney and MEFs, so *Ift20* was selected for our subsequent experiments.

Influence of Mxi1 Transient Overexpression on Ift20 Expression and Ciliogenesis in $Mxi1^{-/-}$ MEFs—To confirm that *Mxi1* regulates *Ift20* expression, we compared *Ift20* expression in *Mxi1* transiently overexpressed $Mxi1^{-/-}$ MEFs and $Mxi1^{-/-}$ MEFs (Fig. 4*A*). When *Mxi1* was transfected into $Mxi1^{-/-}$ MEFs, *Mxi1* (48.721 ± 11.301) and *Ift20* (1.867 ± 0.056) mRNA levels were increased compared with that in $Mxi1^{-/-}$ MEFs. These results indicate that Mxi1 is a positive regulator of Ift20. When *Mxi1* was transfected into $Mxi1^{-/-}$ MEFs, ciliated cells of $Mxi1^{-/-}$ MEFs were increased as indicated by *arrows* com-

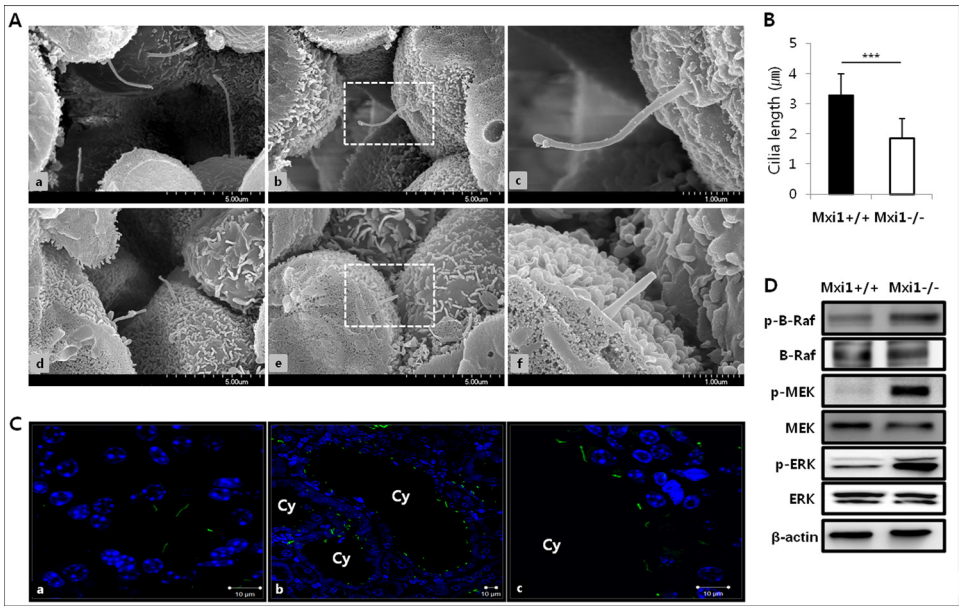

FIGURE 1. **Identification of primary cilium in kidney of *Mxi1*-deficient mice.** *A*, representative photographs of scanning electron micrographs of kidneys from wild-type (*a–c*), aged 9 months, and *Mxi1*-deficient kidney (*d–f*) as age-matched controls. *B*, comparison of the length of cilium in *Mxi1*-deficient kidney with wild-type kidney. The length of cilium was quantified by measuring from ciliary tip to basal body (basal body is bottom and protruding region of cilia) using the *scale bar* indicated in the figure. The graph shows mean ± S.D. (*error bars*) of three independent experiments. The one-tailed *p* value is <0.0001, considered extremely significant (***). *C*, representative photographs of anti-acetylated α-tubulin-stained *Mxi1*-deficient kidney (*b* and *c*) and wild-type kidney (*a*) (anti-acetylated α-tubulin staining (*green*), DAPI staining (*blue*), *Cy*, cyst. Original magnification, ×3000. *Scale bars*, 10 μm. *D*, Western blot of proteins related to B-Raf/MEK/ERK pathway in *Mxi1*-deficient kidney and wild-type. β-Actin was used as a loading control.

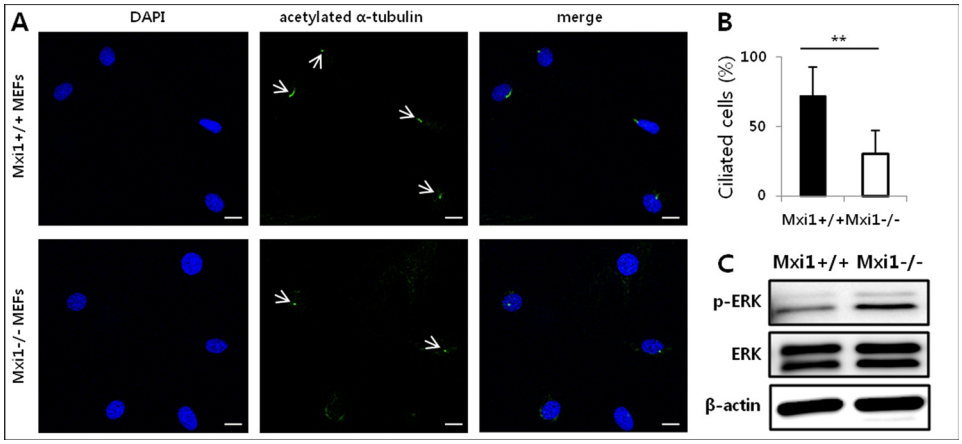

FIGURE 2. **Effect of Mxi1 on ciliogenesis and *p*-ERK level in MEFs.** *A*, representative photographs of anti-acetylated α-tubulin-stained $Mxi1^{+/+}$, $Mxi1^{-/-}$ MEFs. *White arrow* indicates cilia stained with anti-acetylated α-tubulin. Anti-acetylated α-tubulin staining is shown in *green*, DAPI staining is *blue*. Original magnification, ×400. *Scale bar*, 20 μm. *B*, quantification of ciliated cells in $Mxi1^{+/+}$, $Mxi1^{-/-}$ MEFs. To measure ciliated cells, a ratio of the number of cilia to the number of nuclei was calculated and multiplied by 100. The graph shows mean ± S.D. (*error bars*) of three independent experiments. The one-tailed *p* value is < 0.001, considered extremely significant (**). *C*, Western blot of *p*-ERK and total ERK in $Mxi1^{+/+}$ and $Mxi1^{-/-}$ MEFs. β-Actin was used as a loading control.

pared with $Mxi1^{-/-}$ MEFs, suggesting that *Mxi1* transfection increased ciliogenesis of $Mxi1^{-/-}$ MEFs (Fig. 4*B*). Quantification of ciliated cells in $Mxi1^{-/-}$ ($n = 20$, 31.909 ± 6.421%) and *Mxi1* transiently overexpressed $Mxi1^{-/-}$ MEFs ($n = 13$, 54.047 ± 11.16%) is described in Fig. 4*C*. Additionally, *p*-ERK level was measured in $Mxi1^{+/+}$ MEFs, $Mxi1^{-/-}$ MEFs, and *Mxi1* transiently overexpressed $Mxi1^{-/-}$ MEFs (Fig. 4*D*). When *Mxi1* was transfected into $Mxi1^{-/-}$ MEFs, *p*-ERK level was decreased compared with $Mxi1^{-/-}$ MEFs and similar to that in $Mxi1^{+/+}$ MEFs. These results indicated that *Mxi1* overexpression can rescue $Mxi1^{-/-}$ MEFs from the ciliary-defective phenotype, such as abnormal ciliogenesis and the *p*-ERK level.

Mxi1 Regulates Ift20 Expression and Its Promoter Activity in mIMCD-3 Cells—Next, we used mIMCD-3 cells to identify the effect of Mxi1 on cilia assembly in renal epithelial cells. We verified the expression of *Mxi1* and *Ift20* in mIMCD-3 cells, *Mxi1* transiently overexpressed mIMCD-3 cells, and *Mxi1* siRNA-treated mIMCD-3 cells. *Mxi1* mRNA expression was up-regulated in *Mxi1* transiently overexpressed mIMCD-3 cells (12.397 ± 2.923) and down-regulated in *Mxi1* siRNA-treated mIMCD-3 cells (0.381 ± 0.046) compared with each control. *Ift20* mRNA expression was increased in *Mxi1* transiently overexpressed mIMCD-3 cells (1.532 ± 0.236) and decreased in *Mxi1* siRNA-treated mIMCD-3 cells (0.670 ± 0.170) compared with each control (Fig. 5*A*). Consistent with

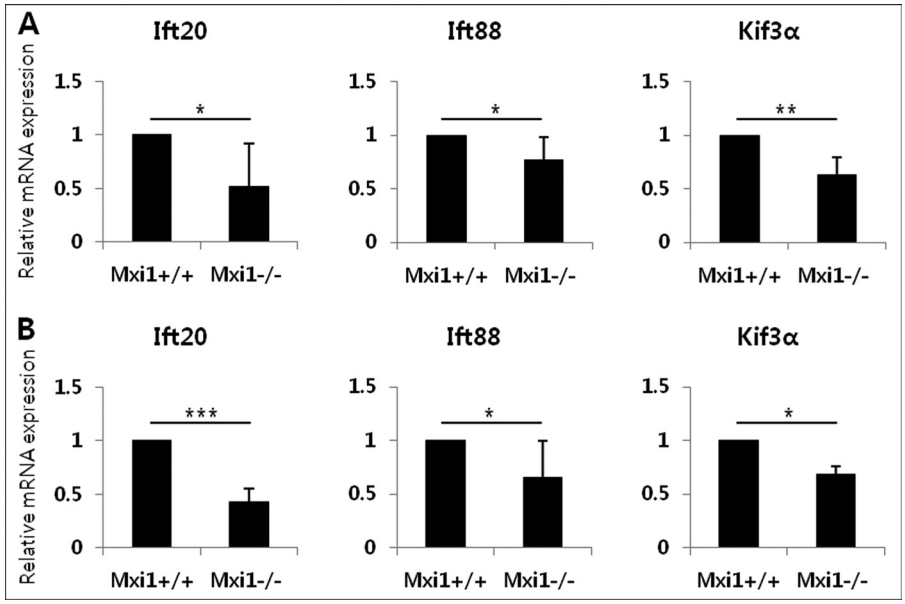

FIGURE 3. **Influence of *Mxi1* inactivation on IFT-related gene expression.** *A*, verification of *Ift20*, *Ift88*, and *Kif3α* mRNA expression in *Mxi1*-deficient mice. The graphs show mean ± S.D. (*error bars*) of three independent experiments. *, $p < 0.05$; **, $p < 0.01$. *B*, verification of *Ift20*, *Ift88*, and *Kif3α* mRNA expression in *Mxi1*-deficient MEFs. The graphs show mean ± S.D. of three independent experiments. *, $p < 0.05$; ***, $p < 0.005$.

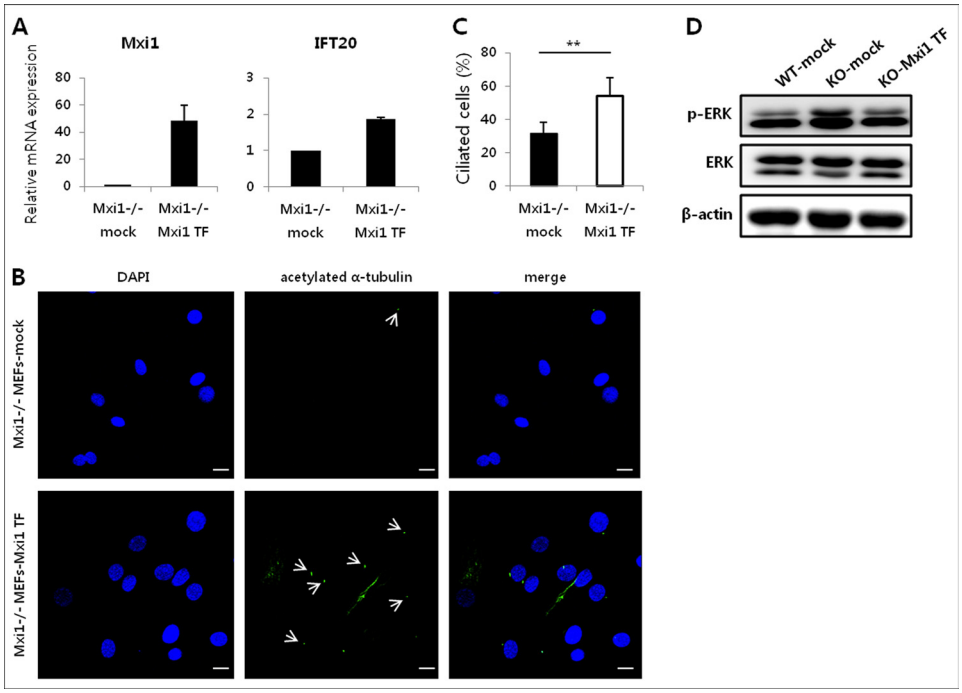

FIGURE 4. **Transient overexpression of *Mxi1* has an effect on ciliary phenotype of *Mxi1*$^{-/-}$ MEFs.** *A*, verification of *Mxi1* and *Ift20* mRNA expression in *Mxi1*$^{-/-}$ and *Mxi1* transiently overexpressed *Mxi1*$^{-/-}$ MEFs. The graphs show mean ± S.D. (*error bars*) in triplicate. *B*, representative photographs of anti-acetylated α-tubulin-stained *Mxi1*$^{-/-}$ and *Mxi1* transiently overexpressed *Mxi1*$^{-/-}$ MEFs. *White arrows* indicates cilia stained with anti-acetylated α-tubulin. Original magnification, ×400. *Scale bars*, 20 μm. *C*, quantification of ciliated cells in *Mxi1*$^{-/-}$ and *Mxi1* transiently overexpressed *Mxi1*$^{-/-}$ MEFs. To measure ciliated cells, the ratio of the number of cilia to the number of nuclei was calculated and multiplied by 100. The graph shows mean ± S.D. of three independent experiments. The one-tailed *p* value is 0.007, considered significant (**). *D*, Western blot of *p*-ERK and total ERK in *Mxi1*$^{+/+}$, *Mxi1*$^{-/-}$, and *Mxi1* transiently overexpressed *Mxi1*$^{-/-}$ MEFs. β-Actin was used as a loading control.

this, Ift20 protein level was regulated by Mxi1 protein level (Fig. 5*B*). Therefore, we found that Ift20 expression was regulated by Mxi1 expression. Next, we confirmed whether Mxi1 regulates *Ift20* promoter activity because Mxi1 is a basic helix-loop-helix leucine zipper transcription factor. We performed a transient transfection assay, in which luciferase reporter constructs driven by various lengths of the *Ift20* 5′-flanking region (−0.5 kb, −1.0 kb, −1.5 kb, and −2.0 kb) in mIMCD-3 cells and *Mxi1* transiently overexpressed mIMCD-3 cells (data not shown). Promoter activity of the −0.5-kb construct increased in *Mxi1* transiently overexpressed mIMCD-3 cells (6.563 ± 1.198) compared with mIMCD-3 cells (2.935 ± 0.553). Promoter activity of the −1.0-kb construct increased in *Mxi1* transiently overexpressed mIMCD-3 cells (5.0223 ± 1.026) compared with

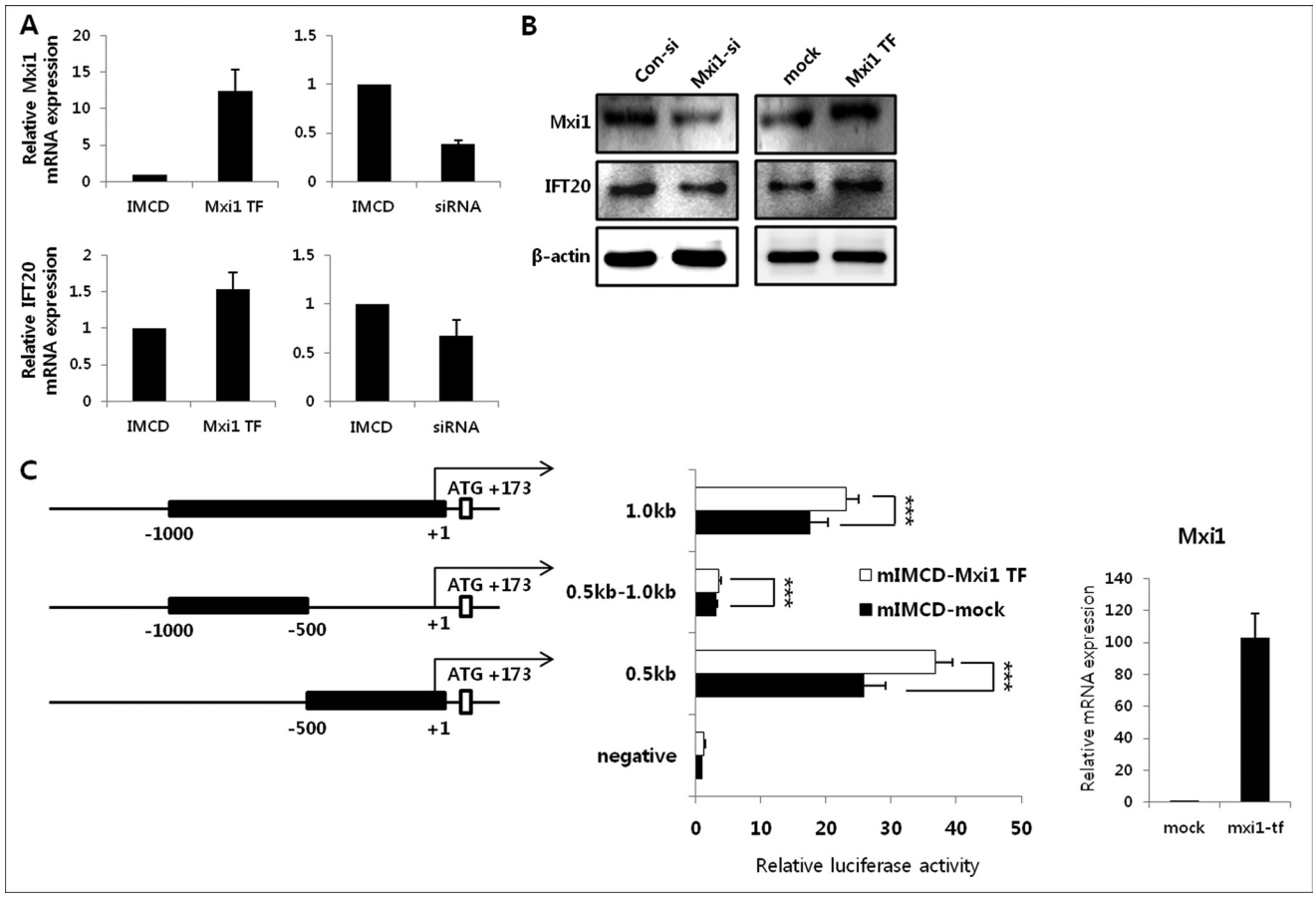

FIGURE 5. **Influence of Mxi1 on Ift20 expression and its promoter activity.** *A*, verification of *Mxi1* and *Ift20* mRNA expression in mIMCD-3 cells (controls), *Mxi1* transiently overexpressed mIMCD-3 cells, and *Mxi1* siRNA-treated mIMCD-3 cells. The graphs show mean ± S.D. (*error bars*) in triplicate. *B*, Western blot of Ift20 and Mxi1 level in *Mxi1* siRNA-treated mIMCD-3 cells and *Mxi1* transiently overexpressed mIMCD-3 cells compared with that in their respective controls. β-Actin was used as a loading control. *C*, deletion constructs of the *Ift20* 5′-flanking region and luciferase activity in mIMCD-3 and *Mxi1* transiently overexpressed mIMCD-3 cells. The representative graph shows mean ± S.D. of three independent assays. ***, $p < 0.005$. The *right part* of the luciferase assay shows *Mxi1* mRNA expression in *Mxi1* transiently overexpressed mIMCD-3 cells compared with that in control used in this luciferase assay. The graph shows mean ± S.D. in triplicate.

mIMCD-3 cells (1.7823 ± 0.303). Promoter activity of the −1.5-kb construct increased in *Mxi1* transiently overexpressed mIMCD-3 cells (3.041 ± 0.475) compared with mIMCD-3 cells (0.902 ± 0.103). Promoter activity of the −2.0-kb construct increased in *Mxi1* transiently overexpressed mIMCD-3 cells (2.933 ± 0.664) than mIMCD-3 cells (0.903 ± 0.276). This luciferase assay shows that promoter activities with the −0.5 kb, −1.0 kb, −1.5 kb, and −2.0 kb were increased in *Mxi1* transiently overexpressed mIMCD-3 cells compared with mIMCD-3 cells. Interestingly, the shortest fragment of −0.5 kb displayed the highest luciferase activity among various fragments, which suggested the presence of positive regulatory elements in the −0.5-kb region of the *Ift20* promoter. From these reasons, −0.5-kb fragment of *Ift20* promoter was selected for our subsequent experiments. *Mxi1* mRNA level of mIMCD-3 cells used in this promoter activity measurement was described in the *right* part of Fig. 5*C* as a qPCR graph. To confirm whether the −0.5-kb region was critical for *Ift20* promoter regulation related to Mxi1, we designed the +1 to −0.5-kb deleted luciferase reporter (0.5kb-1.0kb) construct and checked activity with −0.5 kb and −1.0 kb (Fig. 5*C*). As a result, *Ift20* promoter activity of the 0.5-kb construct increased in *Mxi1* transiently overexpressed mIMCD-3 cells (36.747 ± 2.681) compared with mIMCD-3 (25.773 ± 3.39). Promoter activity of the 1.0-kb construct increased in *Mxi1* transiently overexpressed mIMCD-3 cells (23.131 ± 1.94) compared with mIMCD-3 cells (17.583 ± 2.772). However, *Ift20* promoter activity in each cell line using 0.5kb-1.0kb was significantly low. These results indicated that Mxi1 may play a positive regulator in the transcriptional regulation of the −0.5-kb region of *Ift20* promoter.

Ciliogenesis Is Regulated by Mxi1 in mIMCD-3 Cells—We imaged ciliated cells in mIMCD-3 and *Mxi1* siRNA-treated mIMCD-3 to confirm whether Ift20 regulated by Mxi1 has an effect on mIMCD-3 ciliogenesis. mIMCD-3 cells treated with control siRNA have many ciliated cells, as indicated by *arrows* in Fig. 6*A*. However, knockdown of *Mxi1* using siRNA reduced the number of ciliated cells (Fig. 6*A*). Quantification of ciliated cells in *Mxi1* siRNA-treated mIMCD-3 ($n = 12$, 15.050 ± 13.799%) and control siRNA-treated mIMCD-3 cells ($n = 12$, 39.026 ± 4.541%) is depicted in Fig. 6*B*. In addition, the *p*-ERK level increased in *Mxi1* siRNA-treated mIMCD-3 compared with that in controls (Fig. 6*C*). These results show that ciliogenesis defects affected by inactivating Mxi1 induce *p*-ERK in mIMCD-3 cells.

Mxi1 Regulates the Ift20 Promoter via Ets-1—Given the previous demonstration that Mxi1 regulates *Ift20* promoter activ-

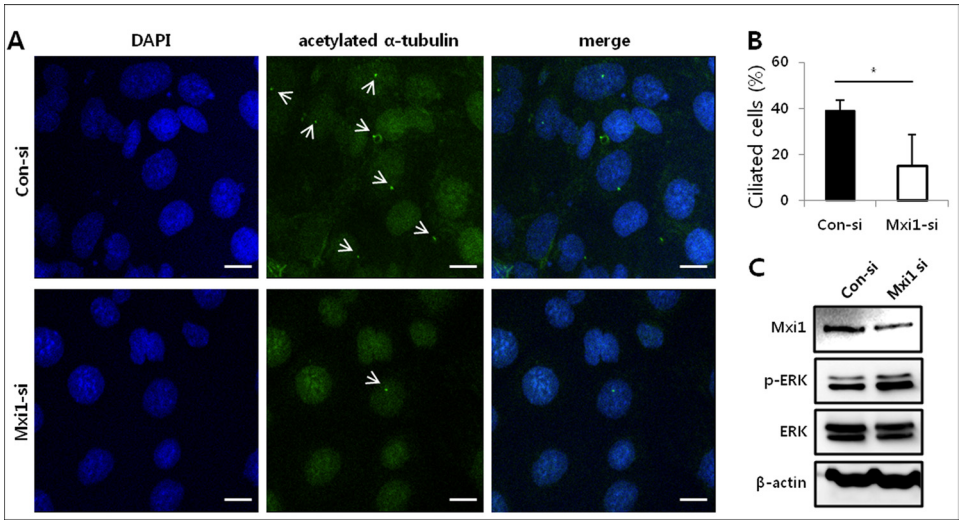

FIGURE 6. **Effect of Mxi1 on ciliogenesis and *p*-ERK level in mIMCD-3 cells.** *A*, representative photographs of anti-acetylated α-tubulin-stained mIMCD-3 cells and *Mxi1* siRNA-treated mIMCD-3 cells. *White arrows* indicate cilia stained with anti-acetylated α-tubulin. Original magnification, ×1200. *Scale bars*, 10 μm. *B*, quantification of ciliated cells in control siRNA-treated and *Mxi1* siRNA-treated mIMCD-3 cells. To measure ciliated cells, a ratio of the number of cilia to the number of nuclei was calculated and multiplied by 100. The graph shows mean ± S.D. (*error bars*) of three independent experiments. The one-tailed *p* value is 0.0263, which was considered significant (*). *C*, Mxi1, *p*-ERK, and total ERK protein levels in mIMCD-3 and *Mxi1* siRNA-treated mIMCD-3 cells. β-Actin was used as the loading control.

ity, we tested whether Mxi1 had a direct or indirect effect on *Ift20* promoter regulation. To identify the transcription factors that bind to the *Ift20* promoter, we screened the consensus binding site for known transcription factors using the TRANSFAC database within the +1 to −0.5-kb region. Transcription factors with high scores were selected and described in Fig. 7*A*. No consensus binding site for Mxi1 was found in the *Ift20* promoter region (−0.5 kb), prompting our prediction that Mxi1 does not directly bind but affects *Ift20* promoter activity indirectly. We performed an electrophoretic mobility shift assay (EMSA) of the consensus binding sites obtained from the TRANSFAC database (data not shown) to identify candidate proteins because we expected that Mxi1 affects *Ift20* promoter activity through a candidate protein that binds to the *Ift20* promoter. Among various transcription factors, Ets-1 was selected as a candidate for binding to the *Ift20* promoter, −135 to −138. A strong shifted band (DNA-protein complex) was detected in the wild-type probe (*lane 3*) containing the Ets-1 binding site (Fig. 7*B*). In addition, the density of this complex decreased dramatically following incubation with the mutant probe (*lane 4*) containing the Ets-1 binding site mutant sequence. A supershift assay was carried out using the Ets-1 antibody to confirm whether this DNA-protein complex contained the Ets-1 protein (Fig. 7*B*). The DNA-protein complex band was diminished (*lane 6*) compared with that in IgG-incubated samples used as a negative control (*lane 5*). Next, we checked *Ift20* promoter activity in *Ets-1* transiently overexpressed mIMCD-3 cells to identify whether Ets-1 had an effect on *Ift20* promoter regulation. *Ets-1* expression level of mIMCD-3 used in this promoter activity measurement is described in the *right part* of the luciferase assay graph in Fig. 7*C*. Luciferase activity increased in *Ets-1* transiently overexpressed mIMCD-3 cells (4.995 ± 1.017) compared with that in controls (2.9 ± 0.205) (Fig. 7*C*), and this increased activity decreased in mutant luciferase constructs (2.644 ± 0.919) containing the mutant Ets-1 binding site sequence despite Ets-1 overexpression (Fig. 7*C*). Consistent with this promoter regulation, the Ift20 protein level decreased in *Ets-1* siRNA-treated mIMCD-3 cells (Fig. 7*D*) compared with that in controls. These results show that Ets-1 binds to −135 to −138 of the *Ift20* promoter and regulates Ift20 expression and promoter activity in mIMCD-3 cells.

From these results, we predicted that the indirect regulatory mechanism of *Ift20* promoter involved in Mxi1 occurred through Ets-1, so we identified the relationship between Mxi1 and Ets-1. No studies have been conducted on this relationship, so we tested whether Mxi1 could be an upstream regulator of Ets-1. The Ets-1 level increased in *Mxi1* transiently overexpressed mIMCD-3 cells compared with that in controls (Fig. 7*E*), but the Mxi1 level did not change in *Ets-1* transiently overexpressed mIMCD-3 and *Ets-1* siRNA-treated mIMCD-3 cells compared with that in each controls (Fig. 7*F*), suggesting that Mxi1 acted as an upstream regulator of Ets-1. The collective results support the suggestion that Mxi1 regulates *Ift20* promoter activity via Ets-1, which binds to the *Ift20* promoter at −135 to −138.

DISCUSSION

In this study, we have shown that the nonciliary protein Mxi1 is a regulator of primary cilia assembly. Many studies have been conducted about the regulatory mechanism between ciliary proteins and primary cilia (2, 30–33), but these studies did not discuss the relationship between nonciliary proteins and primary cilia. From this aspect, our study is significant because it provides new evidence for the function of a nonciliary protein. *Mxi1*-deficient mice have been considered a PKD animal model, but no sufficient disease-inducing mechanisms have been identified. We identify the mechanism in this study.

Defects in renal primary cilia induce polycystic kidneys via abnormal cell proliferation, and aberrant ciliary gene expression has been observed in cystic kidneys. In addition, proteins

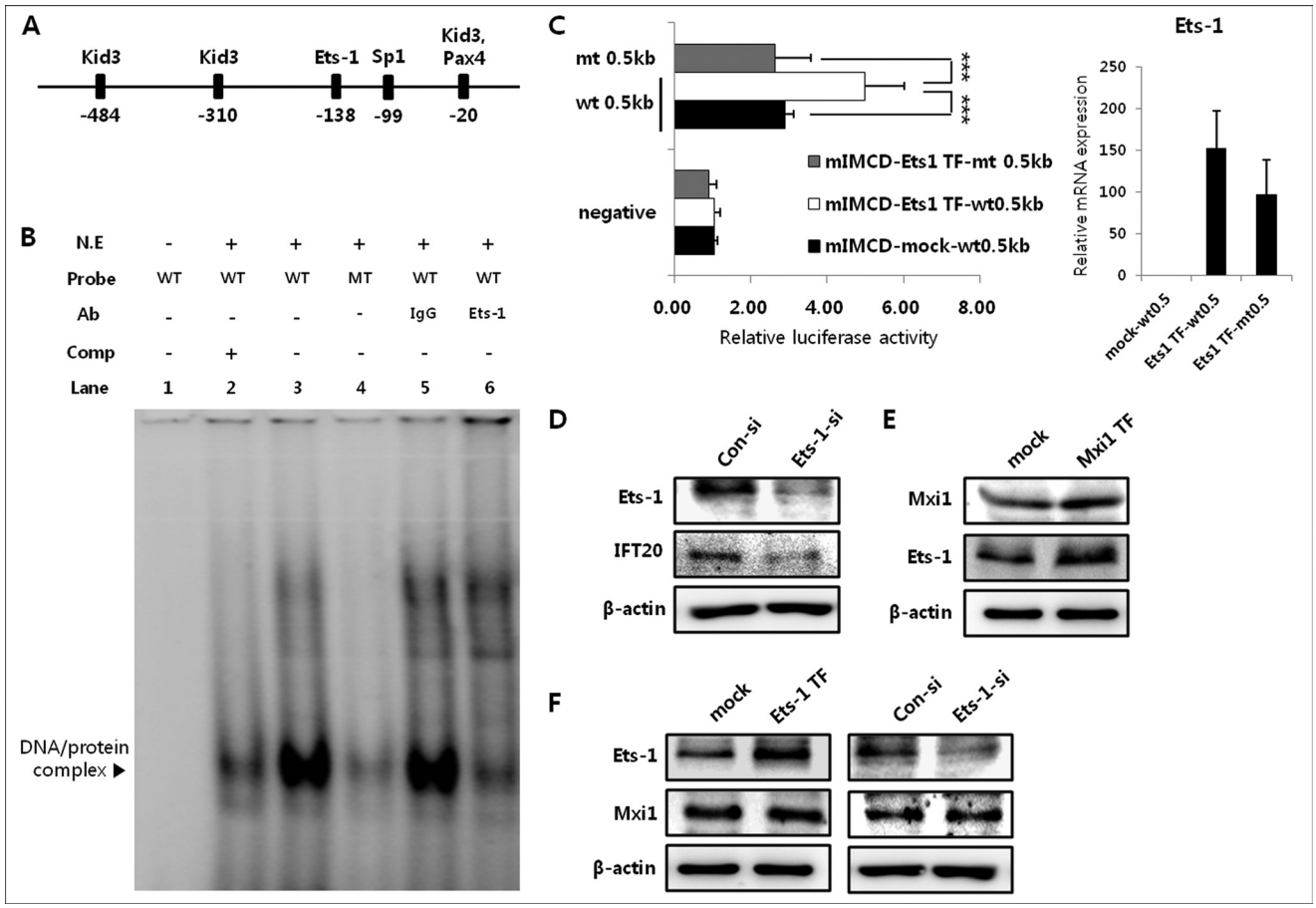

FIGURE 7. **Ets-1 is a mediator of the regulatory mechanism between Mxi1 and Ift20.** *A*, screening of known transcription factors that bind to the *Ift20* promoter using TRANSFAC database. *B*, *lanes 2–4*, gel shift assay. *Lane 6*, supershift assay. *Lane 1*, negative control for the gel shift assay. *Lane 5*, negative control for the supershift assay. *N.E.*, nuclear extracts; *Comp*, competitor. *C*, luciferase assay with construct of 0.5-kb wt (wild-type) and 0.5-kb mt (mutant) containing mutant sequence for the Ets-1 binding site in mIMCD-3 and *Ets-1* transiently overexpressed mIMCD-3. The representative graph shows mean ± S.D. (*error bars*) of three independent assays. ***, $p < 0.005$. The *right part* of the luciferase assay graph indicates *Ets-1* mRNA expression in mock (0.5-kb wt), *Ets-1* transiently overexpressed (TF) 0.5-kb wt, and *Ets-1* transiently overexpressed (TF) 0.5-kb mt transfected mIMCD-3 cells used in this luciferase assay. The graph shows mean ± S.D. in triplicate. *D*, Western blot of Ets-1 and Ift20 protein levels in mIMCD-3 and *Ets-1* siRNA-treated mIMCD-3 cells. β-Actin was used as a loading control. *E*, Mxi1 and Ets-1 protein levels in *Mxi1* transiently overexpressed mIMCD-3 and mIMCD-3 cells. β-Actin was used as a loading control. *F*, Ets-1 and Mxi1 protein levels in mIMCD-3 cells, *Ets-1* transiently overexpressed mIMCD-3 cells, and *Ets-1* siRNA-treated mIMCD-3 cells.

encoded by *Pkd1* and *Pkd2* are main targets of polycystic kidney (34), and these proteins localize to renal cilia to regulate intracellular signaling pathways. Many proteins whose functions are disrupted in cystic kidney disease have been localized to the cilium (5), so cilia and ciliary proteins are considered key components of polycystic kidney. The first discoveries of the relationship between primary cilia and polycystic kidney were demonstrated in Oak Ridge Polycystic Kidney (Orpk) mice, which is mutated in the *Tg737* gene and is a known ortholog of *Chlamydomonas Ift88* (33). Indeed, malformation of primary cilia and abnormalities are observed in Orpk mice. Based on these findings, renal cystic phenotypes are observed in various ciliary gene-targeted mice, so these mice are considered as PKD model. In previous work from our laboratory, we found that inactivating *Mxi1* leads to the formation of numerous renal cysts (25). Additionally, inflammation and abnormal cell proliferation accompanied by renal cysts are observed in the *Mxi1*-deficient kidney (22, 26).

Here, we explain the relationship between *Mxi1* inactivation and cilia disassembly in *Mxi1*-deficient mice, which occurs in renal cysts, because the relevance between cilia defects and ADPKD was recently reported. We observed ciliary defects in *Mxi1*-deficient kidneys and MEFs, so we assumed that Mxi1 had an effect on renal cilia formation. Furthermore, Ift20, a complex B subunit, was the focus of this study to identify the relationship between the cilia defect and *Mxi1* inactivation, because *Ift20* expression is reduced in *Mxi1*-deficient mice and MEFs. Ift20 is required for embryonic viability, and *Ift20* deletion in kidney collecting ducts leads to cystic kidney disease (31). Based on this reference, we expected that abnormal Ift20 expression would play a critical role in renal cyst formation through ciliary defects. Various promoter experiments were performed to demonstrate the mechanism related to Mxi1 and Ift20 regulation, and we found that Ets-1, which binds to the *Ift20* promoter, is a mediator of this mechanism.

Ets-1 is a member of the Ets family of transcription factors and regulates various cellular signaling pathways related to proliferation, differentiation, and apoptosis (35). Few studies have been conducted about the relationship between Ets-1 and polycystic kidney or renal cilia, but it has been reported that Ets factors regulate the *Pkd1* gene promoter (35) localized in renal cilia. We provide the new possibility that Ets-1 is a regulator of

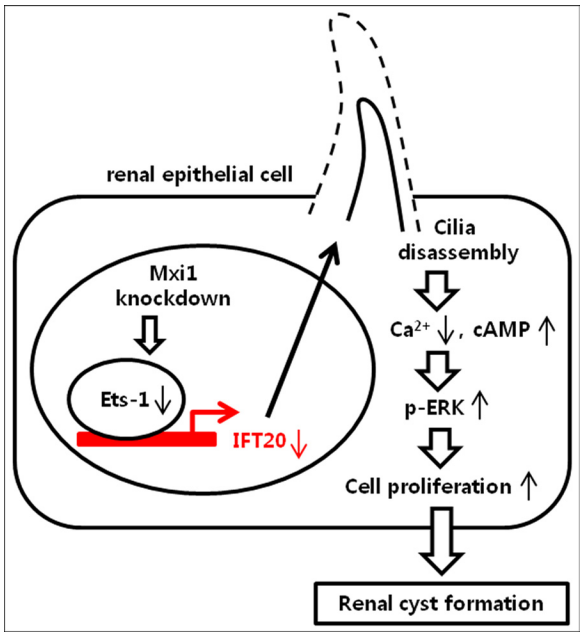

FIGURE 8. **Proposed model illustrating links between inactivation of Mxi1 and renal cyst formation induced by cilia disassembly.** Inactivation of Mxi1 decreases the level of Ets-1, which binds to the *Ift20* promoter. Down-regulation of Ets-1 reduces Ift20 expression and induces cilia disassembly in renal epithelial cells. This abnormal cilia phenotype increases the *p*-ERK level and causes renal cyst formation.

the *Ift20* promoter in this study. From these findings, we expect that Ets-1 is related to polycystic kidney, but further studies are needed.

The collective data support a new model of renal cilia formation regulated by Mxi1 (Fig. 8). Our study is meaningful in revealing a new mechanism from three aspects. First, the renal cilia abnormality is caused by inactivation of the Mxi1. Second, Ets-1 acts as an *Ift20* regulator and is associated with polycystic kidney. Third, Mxi1 is an upstream regulator of Ets-1. Therefore, we suggest that Mxi1 regulates Ift20 expression via Ets-1, which binds to the *Ift20* promoter and has an effect on renal ciliogenesis.

REFERENCES

1. Satir, P., and Christensen, S. T. (2008) Structure and function of mammalian cilia. *Histochem. Cell Biol.* **129,** 687–693
2. Zuo, X., Fogelgren, B., and Lipschutz, J. H. (2011) The small GTPase Cdc42 is necessary for primary ciliogenesis in renal tubular epithelial cells. *J. Biol. Chem.* **286,** 22469–22477
3. Serra, R. (2008) Role of intraflagellar transport and primary cilia in skeletal development. *Anat. Rec.* **291,** 1049–1061
4. Blacque, O. E., Cevik, S., and Kaplan, O. I. (2008) Intraflagellar transport: from molecular characterisation to mechanism. *Front. Biosci.* **13,** 2633–2652
5. Veland, I. R., Awan, A., Pedersen, L. B., Yoder, B. K., and Christensen, S. T. (2009) Primary cilia and signaling pathways in mammalian development, health and disease. *Nephron Physiol.* **111,** p39–53
6. Pedersen, L. B., Veland, I. R., Schrøder, J. M., and Christensen, S. T. (2008) Assembly of primary cilia. *Dev. Dyn.* **237,** 1993–2006
7. Wagner, C. A. (2008) News from the cyst: insights into polycystic kidney disease. *J. Nephrol.* **21,** 14–16
8. Brueckner, M. (2007) Heterotaxia, congenital heart disease, and primary ciliary dyskinesia. *Circulation* **115,** 2793–2795
9. Badano, J. L., Mitsuma, N., Beales, P. L., and Katsanis, N. (2006) The ciliopathies: an emerging class of human genetic disorders. *Annu. Rev. Genomics Hum. Genet.* **7,** 125–148
10. Kennedy, M. P., Omran, H., Leigh, M. W., Dell, S., Morgan, L., Molina, P. L., Robinson, B. V., Minnix, S. L., Olbrich, H., Severin, T., Ahrens, P., Lange, L., Morillas, H. N., Noone, P. G., Zariwala, M. A., and Knowles, M. R. (2007) Congenital heart disease and other heterotaxic defects in a large cohort of patients with primary ciliary dyskinesia. *Circulation* **115,** 2814–2821
11. Ong, A. C., and Harris, P. C. (2005) Molecular pathogenesis of ADPKD: the polycystin complex gets complex. *Kidney Int.* **67,** 1234–1247
12. Al-Bhalal, L., and Akhtar, M. (2005) Molecular basis of autosomal dominant polycystic kidney disease. *Adv. Anat. Pathol.* **12,** 126–133
13. Reeders, S. T. (1992) Multilocus polycystic disease. *Nat. Genet.* **1,** 235–237
14. Torres, V. E., and Harris, P. C. (2006) Mechanisms of disease: autosomal dominant and recessive polycystic kidney diseases. *Nat. Clin. Pract. Nephrol.* **2,** 40–55
15. Park, E. Y., Woo, Y. M., and Park, J. H. (2011) Polycystic kidney disease and therapeutic approaches. *BMB Rep.* **44,** 359–368
16. Pazour, G. J., and Rosenbaum, J. L. (2002) Intraflagellar transport and cilia-dependent diseases. *Trends Cell Biol.* **12,** 551–555
17. Watnick, T., and Germino, G. (2003) From cilia to cyst. *Nat. Genet.* **34,** 355–356
18. Pazour, G. J. (2004) Intraflagellar transport and cilia-dependent renal disease: the ciliary hypothesis of polycystic kidney disease. *J. Am. Soc. Nephrol.* **15,** 2528–2536
19. Kawamata, N., Sugimoto, K. J., Sakajiri, S., Oshimi, K., and Koeffler, H. P. (2005) Mxi1 isoforms are expressed in hematological cell lines and normal bone marrow. *Int. J. Oncol.* **26,** 1369–1375
20. Schreiber-Agus, N., and DePinho, R. A. (1998) Repression by the Mad-(Mxi1)-Sin3 complex. *Bioessays* **20,** 808–818
21. Henriksson, M., and Lüscher, B. (1996) Proteins of the Myc network: essential regulators of cell growth and differentiation. *Adv. Cancer Res.* **68,** 109–182
22. Ko, J. Y., Yoo, K. H., Lee, H. W., and Park, J. H. (2011) Mxi1 regulates cell proliferation through insulin-like growth factor binding protein-3. *Biochem. Biophys. Res. Commun.* **415,** 36–41
23. Wang, D. Y., Xiang, Y. Y., Li, X. J., Hashimoto, M., Tanaka, M., and Sugimura, H. (2000) Mxi1 is a potential cellular target of carcinogens and frequently mutated in experimental rat tumors and tumor cell lines. *Pathol. Int.* **50,** 373–383
24. Schreiber-Agus, N., Meng, Y., Hoang, T., Hou, H., Jr., Chen, K., Greenberg, R., Cordon-Cardo, C., Lee, H. W., and DePinho, R. A. (1998) Role of Mxi1 in ageing organ systems and the regulation of normal and neoplastic growth. *Nature* **393,** 483–487
25. Yoo, K. H., Sung, Y. H., Yang, M. H., Jeon, J. O., Yook, Y. J., Woo, Y. M., Lee, H. W., and Park, J. H. (2007) Inactivation of Mxi1 induces Il-8 secretion activation in polycystic kidney. *Biochem. Biophys. Res. Commun.* **356,** 85–90
26. Yoo, K. H., Kim, Y. N., Lee, M. J., Seong, J. K., and Park, J. H. (2009) Identification of apolipoprotein A1 reduction in the polycystic kidney by proteomics analysis of the Mxi1-deficient mouse. *Proteomics* **9,** 3824–3832
27. Zaucke, F., Boehnlein, J. M., Steffens, S., Polishchuk, R. S., Rampoldi, L., Fischer, A., Pasch, A., Boehm, C. W., Baasner, A., Attanasio, M., Hoppe, B., Hopfer, H., Beck, B. B., Sayer, J. A., Hildebrandt, F., and Wolf, M. T. (2010) Uromodulin is expressed in renal primary cilia, and UMOD mutations result in decreased ciliary uromodulin expression. *Hum. Mol. Genet.* **19,** 1985–1997
28. Salem, H., Rachmin, I., Yissachar, N., Cohen, S., Amiel, A., Haffner, R., Lavi, L., and Motro, B. (2010) Nek7 kinase targeting leads to early mortality, cytokinesis disturbance, and polyploidy. *Oncogene* **29,** 4046–4057
29. Cowley, B. D., Jr. (2008) Calcium, cyclic AMP, and MAP kinases: dysregulation in polycystic kidney disease. *Kidney Int.* **73,** 251–253
30. Keady, B. T., Samtani, R., Tobita, K., Tsuchya, M., San Agustin, J. T., Follit, J. A., Jonassen, J. A., Subramanian, R., Lo, C. W., and Pazour, G. J. (2012) IFT25 links the signal-dependent movement of Hedgehog components to intraflagellar transport. *Dev. Cell* **22,** 940–951
31. Jonassen, J. A., San Agustin, J., Follit, J. A., and Pazour, G. J. (2008) Deletion

of IFT20 in the mouse kidney causes misorientation of the mitotic spindle and cystic kidney disease. *J. Cell Biol.* **183,** 377–384
32. Jonassen, J. A., SanAgustin, J., Baker, S. P., and Pazour, G. J. (2012) Disruption of IFT complex A causes cystic kidneys without mitotic spindle misorientation. *J. Am. Soc. Nephrol.* **23,** 641–651
33. Takiar, V., and Caplan, M. J. (2011) Polycystic kidney disease: pathogenesis and potential therapies. *Biochim. Biophys. Acta* **1812,** 1337–1343
34. Nauli, S. M., Alenghat, F. J., Luo, Y., Williams, E., Vassilev, P., Li, X., Elia, A. E., Lu, W., Brown, E. M., Quinn, S. J., Ingber, D. E., and Zhou, J. (2003) Polycystins 1 and 2 mediate mechanosensation in the primary cilium of kidney cells. *Nat. Genet.* **33,** 129–137
35. Puri, S., Rodova, M., Islam, M. R., Magenheimer, B. S., Maser, R. L., and Calvet, J. P. (2006) Ets factors regulate the polycystic kidney disease-1 promoter. *Biochem. Biophys. Res. Commun.* **342,** 1005–1013

Inactivation of Max-interacting Protein 1 Induces Renal Cilia Disassembly through Reduction in Levels of Intraflagellar Transport 20 in Polycystic Kidney

Je Yeong Ko, Kyung Hyun Yoo, Seon Ah Song, Do Yeon Kim, Hyun Kyung Kong, Curie Ahn, Han Woong Lee, Duk-Hee Kang, Goo Taeg Oh and Jong Hoon Park

J. Biol. Chem. 2013, 288:6488-6497.
doi: 10.1074/jbc.M112.413302 originally published online January 13, 2013
